AMERICAN SOCIETY FOR MICROBIOLOGY | Journal of Virology®

GENETIC DIVERSITY AND EVOLUTION

# Koala and Wombat Gammaherpesviruses Encode the First Known Viral NTPDase Homologs and Are Phylogenetically Divergent from All Known Gammaherpesviruses

Paola K. Vaz,[a] Carol A. Hartley,[a] Sang-Yong Lee,[b] Fiona M. Sansom,[a] Timothy E. Adams,[c] Kathryn Stalder,[a] Lesley Pearce,[c] George Lovrecz,[c] Glenn F. Browning,[a] Christa E. Müller,[b] Joanne M. Devlin[a]

[a]Asia-Pacific Centre for Animal Health, Melbourne Veterinary School, Faculty of Veterinary and Agricultural Sciences, The University of Melbourne, Parkville, Victoria, Australia

[b]PharmaCenter Bonn, Pharmaceutical Institute, Pharmaceutical Chemistry I, University of Bonn, Bonn, Germany

[c]CSIRO Manufacturing, Parkville, Victoria, Australia

**ABSTRACT** There is a large taxonomic gap in our understanding of mammalian herpesvirus genetics and evolution corresponding to those herpesviruses that infect marsupials, which diverged from eutherian mammals approximately 150 million years ago (mya). We compare the genomes of two marsupial gammaherpesviruses, *Phascolarctid gammaherpesvirus 1* (PhaHV1) and *Vombatid gammaherpesvirus 1* (VoHV1), which infect koalas (*Phascolarctos cinereus*) and wombats (*Vombatus ursinus*), respectively. The core viral genomes were approximately 117 kbp and 110 kbp in length, respectively, sharing 69% pairwise nucleotide sequence identity. Phylogenetic analyses showed that PhaHV1 and VoHV1 formed a separate branch, which may indicate a new gammaherpesvirus genus. The genomes contained 60 predicted open reading frames (ORFs) homologous to those in eutherian herpesviruses and 20 ORFs not yet found in any other herpesvirus. Seven of these ORFs were shared by the two viruses, indicating that they were probably acquired prespeciation, approximately 30 to 40 mya. One of these shared genes encodes a putative nucleoside triphosphate diphosphohydrolase (NTPDase). NTPDases are usually found in mammals and higher-order eukaryotes, with a very small number being found in bacteria. This is the first time that an NTPDase has been identified in any viral genome. Interrogation of public transcriptomic data sets from two koalas identified PhaHV1-specific transcripts in multiple host tissues, including transcripts for the novel NTPDase. PhaHV1 ATPase activity was also demonstrated *in vitro*, suggesting that the encoded NTPDase is functional during viral infection. In mammals, NTPDases are important in downregulation of the inflammatory and immune responses, but the role of the PhaHV1 NTPDase during viral infection remains to be determined.

**IMPORTANCE** The genome sequences of the koala and wombat gammaherpesviruses show that the viruses form a distinct branch, indicative of a novel genus within the *Gammaherpesvirinae*. Their genomes contain several new ORFs, including ORFs encoding a $\beta$-galactoside $\alpha$-2,6-sialyltransferase that is phylogenetically closest to poxvirus and insect homologs and the first reported viral NTPDase. NTPDases are ubiquitously expressed in mammals and are also present in several parasitic, fungal, and bacterial pathogens. In mammals, these cell surface-localized NTPDases play essential roles in thromboregulation, inflammation, and immune suppression. In this study, we demonstrate that the virus-encoded NTPDase is enzymatically active and is transcribed during natural infection of the host. Understanding how these enzymes benefit viruses can help to inform how they may cause disease or evade host immune defenses.

**KEYWORDS** NTPDase, genomes, herpesviruses, marsupial, nucleotide metabolism

**Citation** Vaz PK, Hartley CA, Lee S-Y, Sansom FM, Adams TE, Stalder K, Pearce L, Lovrecz G, Browning GF, Müller CE, Devlin JM. 2019. Koala and wombat gammaherpesviruses encode the first known viral NTPDase homologs and are phylogenetically divergent from all known gammaherpesviruses. J Virol 93:e01404-18. https://doi.org/10.1128/JVI.01404-18.

**Editor** Jae U. Jung, University of Southern California



Address correspondence to Paola K. Vaz, pvaz@unimelb.edu.au.

**Received** 13 September 2018
**Accepted** 12 December 2018
**Accepted manuscript posted online** 19 December 2018
**Published** 5 March 2019

Marsupial divergence from eutherian mammals occurred approximately 150 million years ago (mya) (1, 2). Rapid eutherian diversification occurred about 20 million years before that of marsupials (at 82 mya), and this explosive radiation led to the rise of nearly all extant placental orders by 85 mya (1). This period of taxonomic mammalian diversity coincided with, or even drove with it, herpesvirus evolution (3). Herpesviruses are widespread throughout the animal kingdom and can cause disease and death in a wide range of species (4, 5). They are among the largest and most complex of viruses and are superbly well adapted to their hosts, with many examples of their ability to manipulate and bypass host immune and cellular defenses (6).

Herpesvirus-induced disease and mortality in marsupials were first recognized in the mid-1970s, in several macropod species (7–9). Currently, there are 15 distinct marsupial herpesviruses reported, consisting of 4 alphaherpesviruses and 11 gammaherpesviruses, infecting diverse marsupial species (10–16). The clinical significance of many of these viruses remains largely unexplored, but macropodid alphaherpesvirus 1 (MaHV1) and MaHV2 have caused fatal systemic disease and severe clinical signs, including reproductive failure, conjunctivitis, respiratory disease, pyrexia, vesicular anogenital lesions, and hepatic disease, in wild and captive populations of threatened macropods (7–9, 17). The gammaherpesvirus MaHV3 has been associated with ulcerative cloacitis and mammary gland tumors in a captive population of eastern gray kangaroos (EGKs; *Macropus giganteus*) (14) and respiratory disease and mortality in wild EGKs (18). The alphaherpesvirus MaHV4 has been associated with respiratory and possible neurological disease, also in wild EGKs (12).

While a great deal is known about many herpesviruses that infect placental animals, particularly humans and animals of agricultural importance, the first marsupial herpesvirus genome, that of an alphaherpesvirus, was only published in 2016 (19). Studying the genetics of herpesviruses from noneutherian mammals contributes to our understanding of mammalian herpesvirus genetics and evolution. In this study, we focused on the genetics of two metatherian gammaherpesviruses, *Phascolarctid gammaherpesvirus 1* (PhaHV1) from koalas (*Phascolarctos cinereus*) and *Vombatid gammaherpesvirus 1* (VoHV1) from wombats (*Vombatus ursinus*) (11, 13). PhaHV1 was first described in 2011 in three geographically distinct wild koalas that were suffering from other concurrent infections and were showing signs of severe sarcoptic mange, pulmonary congestion, bilateral conjunctivitis, and chronic cystitis, most likely due to *Chlamydia* infection. VoHV1 was first identified in 2015 in a large molecular survey of herpesviruses in marsupial species that included 33 wild wombats, as well as 99 koalas (13). In that study, VoHV1 was detected in 15% of wombats and PhaHV1 was detected in 5% of koalas. The two viruses sequenced in this study both originated from samples collected from wild-caught animals in the 2015 study, specifically, the oropharyngeal swab of a koala and the nasal swab of a bare-nosed wombat.

We compared the genomes of PhaHV1 and VoHV1, with particular attention to their relationship to each other and to the *Gammaherpesvirinae* more generally, and used these data to trace viral dissemination and transcription within the host. We also investigated novel enzymes encoded by the viruses, including their activity *in vitro*.

## RESULTS

**PhaHV1 and VoHV1 whole-genome sequence analysis.** *De novo* assemblies of PhaHV1 and VoHV1 resulted in core genomes (excluding large reiterative repeat regions and genomic termini) of approximately 117 kbp and 110 kbp in length, respectively (Fig. 1; see also Fig. S1 in the supplemental material; GenBank accession numbers MG452721 and MG452722, respectively) and genome G+C values of 45% and 43%, respectively. The sizes of the large tandem repeat regions were not resolved. The final genome assembly of PhaHV1 had a mean depth of 176 reads per bp (0.2 million mapped reads), and approximately 95% of reads had a quality score of at least $Phred_{20}$. VoHV1 had a mean depth of 333 reads per bp (0.3 million mapped reads), and approximately 95% of reads had a quality score of at least $Phred_{20}$.

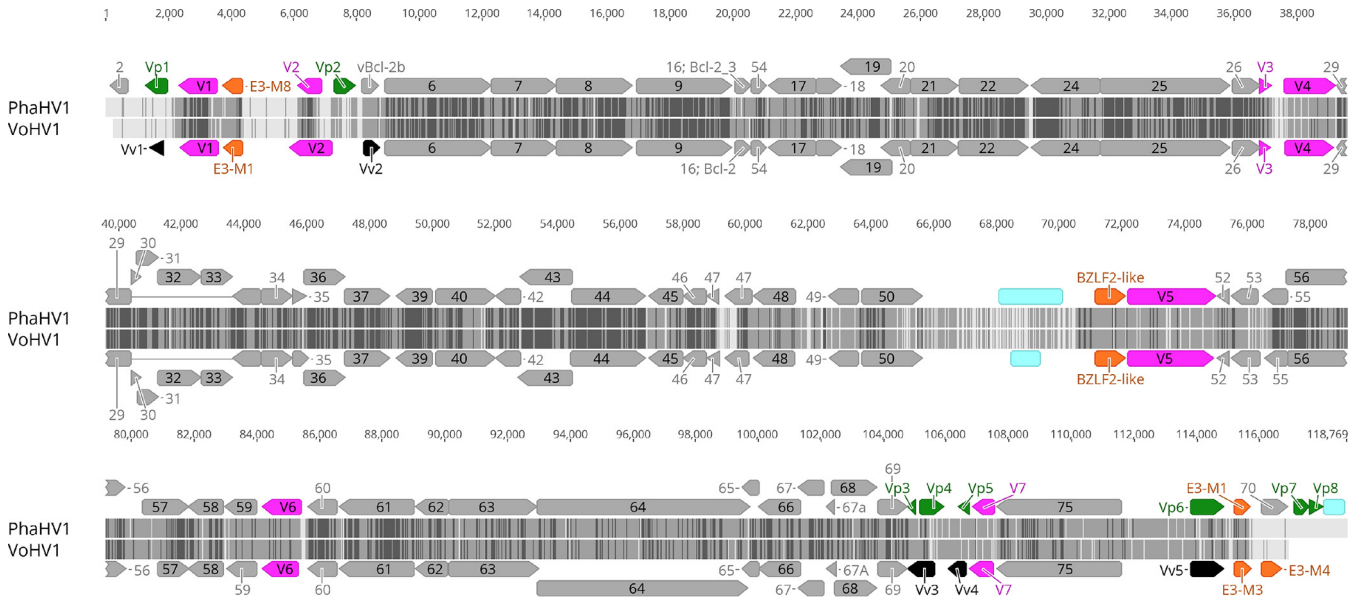


**FIG 1** Whole-genome sequence alignment of PhaHV1 and VoHV1. Conserved genes are annotated in gray using the herpesvirus saimiri (HVS) ORF nomenclature. ORFs colored orange are homologs of genes found in Epstein-Barr virus (BZLF2), Kaposi's sarcoma-associated herpesvirus (E3), or equine gammaherpesvirus 2 (E4). Novel herpesvirus ORFs shared by PhaHV1 and VoHV1 (magenta) are given a V prefix, while virus unique ORFs (green or black) were given a Vp (PhaHV1) or Vv (VoHV1) prefix, and regions of low confidence are pale blue. Increasing nucleotide sequence identity between viral genome sequences is indicated by an increasing darker gray scale: light gray, no identity; medium gray, similar; black, identity; dashes, gap sites. A high-resolution image is provided in Fig. S1 in the supplemental material.

Both genomes had gene arrangements consistent with those of the genomes of other gammaherpesviruses and encoded 60 genes, or open reading frames (ORFs), common to eutherian herpesviruses more generally (Fig. 1; Table 1). The predicted protein sequences of these core genes shared between 44.2% (ORF45; host unknown protein) and 80.2% (ORF60; ribonucleotide reductase small subunit 2) amino acid sequence identity with each other. We also detected homologs of genes identified less commonly in the genomes of herpesviruses, including several E3-like (ubiquitin ligases) (20) and E4-like (viral Bcl-2) (21) ORFs and BZLF2 (22). Phylogenetic relationships with representative members of the *Herpesviridae* were examined using the conserved glycoprotein B (gB) and DNA polymerase (DPOL) herpesvirus genes. PhaHV1 and VoHV1 branched separately from existing genera (Fig. 2 and Table S1).

**Shared novel hypothetical ORFs in PhaHV1 and VoHV1.** Seven ORFs shared by both viruses (annotated V1 to V7) were either novel or not previously found in herpesviruses. No putative functional domains or motifs were identified in ORF V2, V3, V5, or V7. GenBank and Conserved Domain Database (CDD) searches identified putative functions for ORFs V1 (Pfam00777, $\beta$-galactoside $\alpha$-2,6-sialyltransferase 1 [ST6Gal1]), V4 (Pfam01150, nucleoside triphosphate diphosphohydrolase [NTPDase]), and V6 (Pfam04929, DNA replication accessory factor, which may be a distant ORF59 paralog), and these predicted putative functions were supported by structural prediction analysis with the I-TASSER server. The V4 homologs in both viruses shared 39.3% pairwise amino acid sequence identity (69% nucleotide sequence identity) and shared up to 36% amino acid sequence identity with NTPDases of vertebrates. NTPDases catalyze the conversion of nucleoside triphosphates to di- and monophosphates, most commonly converting ATP to ADP and AMP. In PhaHV1, V4 contained all five apyrase conserved regions (ACRs), including conserved residues necessary for enzymatic function (Fig. 3A), as well as conserved cysteines important for tertiary structure (23). The identification of two putative transmembrane domains (TMDs) suggests that the enzyme was membrane bound. Localization predictions indicate that it is likely to be cell surface located, with the catalytic site facing the extracellular milieu and the N and C termini being found within the cytoplasm, although localization to the membrane of intracellular

**TABLE 1** Predicted ORFs identified within the assembled core genomes of PhaHV1 and VoHV1 and their amino acid pairwise sequence identities[a]

| Gene | Description (putative) | Length (nt) | | Amino acid sequence identity (%) for PhaHV1 and VoHV1 |
|---|---|---|---|---|
| | | PhaHV1 | VoHV1 | |
| ORF2 | Dihydrofolate reductase (DHFR) | 588 | | |
| ORF6 | Single-stranded DNA-binding protein | 3,381 | 3,384 | 72.4 |
| ORF7 | Terminase subunit; capsid associated | 2,040 | 2,046 | 63.7 |
| ORF8 | gB | 2,430 | 2,415 | 75.2 |
| ORF9 | Catalytic subunit of the DNA polymerase complex | 3,036 | 3,027 | 77.1 |
| ORF16 | Bcl-2 homolog; antiapoptotic activity | 507 | 507 | 42.0 |
| ORF17 | Serine protease; maturation of scaffold proteins | 1,467 | 1,479 | 55.2 |
| ORF18 | Unknown | 825 | 831 | 57.6 |
| ORF19 | Portal capping protein | 1,593 | 1,635 | 66.5 |
| ORF20 | Nuclear protein | 876 | 927 | 44.3 |
| ORF21 | Thymidine kinase | 1,533 | 1,485 | 61.3 |
| ORF22 | gH; complexed with gN | 2,196 | 2,223 | 74.7 |
| ORF24 | Unknown | 2,172 | 2,202 | 64.4 |
| ORF25 | Major capsid protein | 4,140 | 4,140 | 76.5 |
| ORF26 | Capsid triplex subunit | 912 | 912 | 78.9 |
| ORF29a | Terminase ATPase subunit | 1,053 | 1,056 | 80.1 |
| ORF29b | Terminase ATPase subunit | 963 | 948 | 67.0 |
| ORF30 | Interacts with ORF18; role in late gene expression | 309 | 345 | 51.6 |
| ORF31 | BDLF4; unknown | 699 | 681 | 65.5 |
| ORF32 | Tegument protein; capsid localization in the nucleus | 1,371 | 1,359 | 56.5 |
| ORF33 | Interacts with ORF38; regulates ORF36 | 1,020 | 1,020 | 67.8 |
| ORF34 | Interacts with ORF38; regulates ORF36 | 978 | 972 | 64.5 |
| ORF35 | BGLF3.5; unknown | 459 | 519 | 55.7 |
| ORF36 | Tegument protein; serine-threonine protein kinase | 1,341 | 1,326 | 69.5 |
| ORF37 | DNase; DNA maturation and recombination | 1,434 | 1,434 | 73.0 |
| ORF39 | gM: complexed with gN | 1,167 | 1,164 | 74.1 |
| ORF40 | Helicase-primase complex subunit | 1,893 | 1,875 | 47.0 |
| ORF42 | Tegument protein; nuclear egress | 798 | 798 | 63.5 |
| ORF43 | Capsid portal protein | 1,677 | 1,752 | 74.1 |
| ORF44 | Helicase-primase complex subunit | 2,358 | 2,403 | 79.6 |
| ORF45 | Nuclear phosphoprotein | 1,050 | 1,002 | 44.2 |
| ORF46 | Uracil-DNA glycosylase | 753 | 753 | 74.4 |
| ORF47 | gL; complexed with gH | 864 | 528 | 45.8 |
| ORF48 | BRRF2; unknown | 1,320 | 1,332 | 42.1 |
| ORF49 | Transcontrol protein | 960 | 927 | 31.3 |
| ORF50 | R transactivator (RTA) | 1,887 | 1,818 | 44.5 |
| ORF52 | BLRF2; tegument protein, p23 capsid antigen | 411 | 402 | 69.9 |
| ORF53 | gN; complexed with gM | 750 | 919 | 33.1 |
| ORF54 | Deoxyuridine triphosphatase | 498 | 498 | 65.5 |
| ORF55 | Cytoplasmic egress facilitator | 1,098 | 1,215 | 61.8 |
| ORF56 | Helicase-primase complex subunit; primase | 2,553 | 2,520 | 63.9 |
| ORF57 | Transcriptional control factor | 1,470 | 978 | 63.9 |
| ORF58 | Putative integral membrane glycoprotein | 1,098 | 1,092 | 55.3 |
| ORF59 | Processivity subunit of the DNA polymerase complex | 1,062 | 933 | 46.7 |
| ORF60 | Ribonucleotide reductase; small subunit | 932 | 927 | 80.2 |
| ORF61 | Ribonucleotide reductase; large subunit | 2,415 | 2,373 | 68.0 |
| ORF62 | Capsid triplex subunit | 1,032 | 1,017 | 58.8 |
| ORF63 | Tegument protein; interacts with ORF64 | 2,805 | 2,856 | 52.8 |
| ORF64 | Large tegument protein; interacts with ORF63 | 6,741 | 6,723 | 49.3 |
| ORF65 | Small capsid protein; interacts with dynein | 540 | 546 | 49.5 |
| ORF66 | Nuclear egress membrane protein | 1,350 | 1,344 | 64.3 |
| ORF67 | Inner nuclear membrane protein; capsid docking | 834 | 849 | 63.2 |
| ORF67A | Viral DNA genome packaging; viral release | 267 | 324 | 57.5 |
| ORF68 | Capsid transport nuclear protein | 1,433 | 1,362 | 55.8 |
| ORF69 | Nuclear matrix protein; capsid docking | 954 | 951 | 63.6 |
| ORF70 | Thymidylate synthase | 867 | | |
| ORF75 | Large tegument protein/viral FGAM synthase | 3,975 | 3,969 | 49.9 |
| E3-M1 | MARCH1-like homolog; ubiquitin ligase | | 576 | |
| E3-M1/8 | MARCH1/8-like homolog; ubiquitin ligase | 528 | | |
| E3-M3 | MARCH3-like homolog; ubiquitin ligase | | 552 | |
| E3-M4 | MARCH4-like homolog; ubiquitin ligase | | 570 | |
| E3-M8 | MARCH8-like homolog; ubiquitin ligase | 618 | | |
| E4 | Viral Bcl-2; BALF1 homolog | 579 | | |
| BZLF2 | B cell lymphocyte infection factor; envelope glycoprotein | 1,059 | 933 | 35.3 |

(Continued on next page)

**TABLE 1** (Continued)

| Gene | Description (putative) | Length (nt) | | Amino acid sequence identity (%) for PhaHV1 and VoHV1 |
|---|---|---|---|---|
| | | PhaHV1 | VoHV1 | |
| Conserved ORFs within PhaHV1 and VoHV1 | | | | |
| V1 | β-Galactoside α-2,6-sialyltransferase 1 (ST6Gal1) | 1,209 | 1,215 | 56.9 |
| V2 | Hypothetical protein | 756 | 768 | 48.9 |
| V3 | Hypothetical protein | 360 | 360 | 55.8 |
| V4 | Nucleoside triphosphate diphosphohydrolase (NTPDase) | 1,548 | 1,524 | 39.0 |
| V5 | Hypothetical protein | 2,847 | 3,336 | 31.4 |
| V6 | Hypothetical protein; ORF59-like paralog | 1,626 | 1,164 | 47.7 |
| V7 | Hypothetical protein | 627 | 768 | 30.9 |

[a]ORF naming and descriptions follow the convention for gammaherpesvirus, as described previously (21, 67–69). nt, number of nucleotides.

vesicles or organelles is also possible. Similar analysis of the VoHV1 V4 homolog identified well-conserved ACRs 1, 2, 3, and 5 and a second putative ACR3 (ACR3b), but ACR4 contained a number of amino acid changes, importantly, at conserved residues implicated in enzymatic function (D221H, G223D, G224T) (Fig. 3A). The V4 catalytic sites from three additional VoHV1-positive and two PhaHV1-positive animals were also PCR amplified and sequenced. Results showed that all 5 ACRs were identical to those of the isolates whose full genomes were sequenced. Six single nucleotide polymorphisms (SNPs; four of which were nonsynonymous) were identified across two of the three amplified VoHV1 V4 sites, and these were located between ACRs 2 and 3 and between ACRs 4 and 5. No SNPs were detected within PhaHV1 V4. VoHV1 V4 also contained the two putative TMDs identified in PhaHV1 V4. Phylogenetic analysis of the viral NTPDase homologs (Fig. 3B) found that they clustered most closely with the mammalian cell surface-located NTPDases (NTPDases 1 to 3 and 8), despite the low similarity across the whole gene.

The V1 (ST6Gal1) homologs encoded in the genomes of both viruses shared 57% pairwise amino acid sequence identity with each other and shared only up to 37% amino acid sequence identity with the ST6Gal1s of vertebrates. Both homologs contained similar amino acid sequence structural features (Fig. 4A): a putative N-terminal TMD and signal sequence cleavage site and an ST6Gal1 catalytic site, identified by both PFAM and I-TASSER analyses. Additionally, a conserved substrate-binding motif (SSG) was identified. These features suggest that both these ST6Gal1 homologs are likely to be functional. Phylogenetic analysis of the viral ST6Gal1 homologs (Fig. 4B) found that they clustered with the only two other known virally encoded ST6Gal homologs, found in Yoka poxvirus (PV) and squirrel poxvirus (24, 25), although they shared low amino

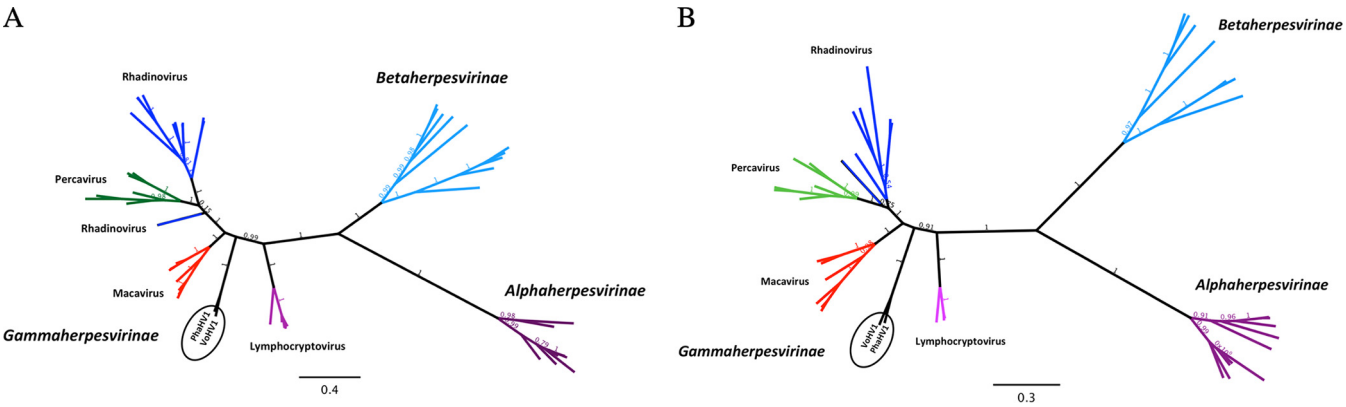


**FIG 2** Phylogenetic relationships between PhaHV1, VoHV1, and other representative herpesviruses using the translated amino acid sequences of two highly conserved genes, glycoprotein B (A) and DNA polymerase (B). The sequences were aligned using the MAFFT plug-in and refined using the ClustalW program. Maximum likelihood trees were built using the Jones-Taylor-Thornton substitution model with 100 bootstrap replicates. Refer to Table S1 in the supplemental material for the list of sequences used for each analysis.

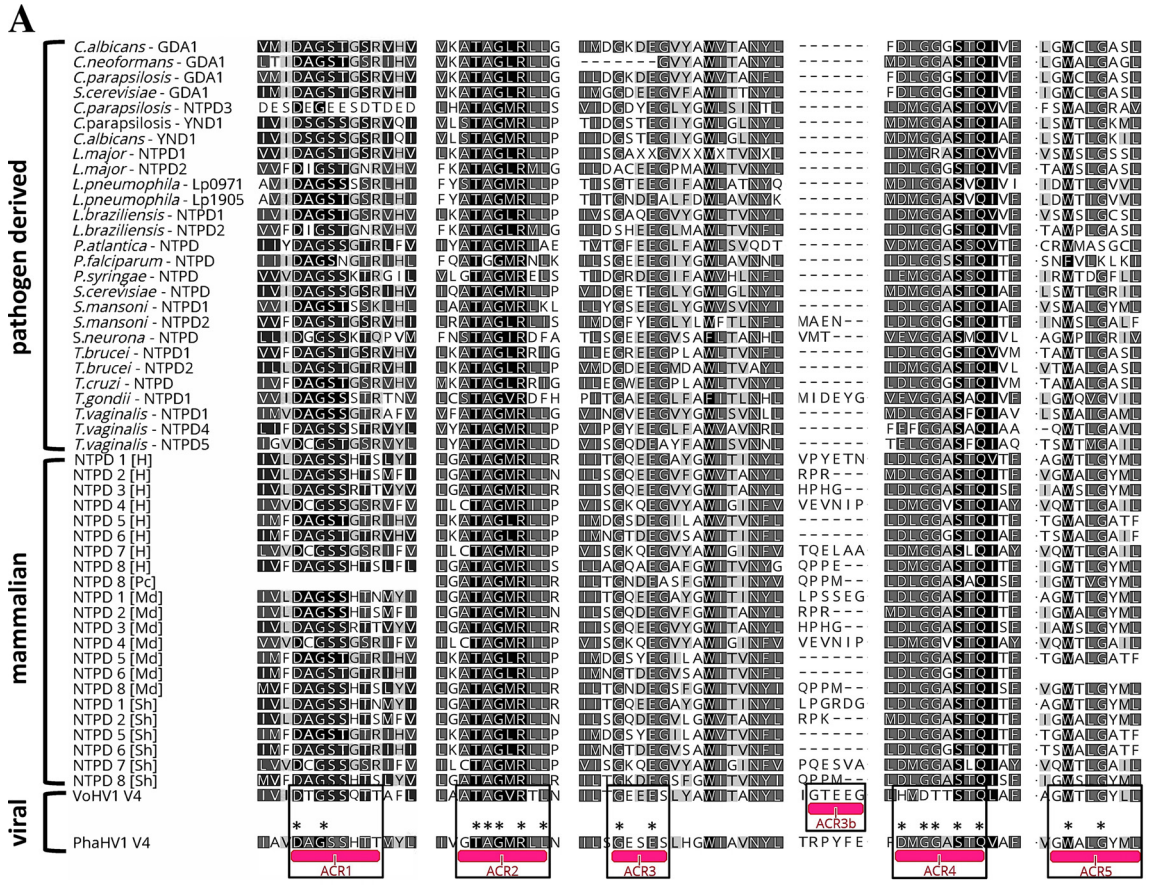


**FIG 3** Phylogenetic comparisons of V4 ORFs from PhaHV1 and VoHV1 with the NTPDases of representative mammalian, bacterial, parasitic, and fungal species. (A) ClustalW alignment of NTPDase apyrase conserved regions 1 to 5 (ACR1 to ACR5, pink underline).

(Continued on next page)

acid sequence similarity (30% pairwise amino acid sequence identity). As a group, the viral homologs clustered with the insect genome-encoded ST6Gal rather than the ST6Gals found in vertebrates (Fig. 4B).

Eight additional hypothetical ORFs (annotated Vp1 to Vp8) were identified only in the PhaHV1 genome, and five unique ORFs (tentatively annotated Vv1 to Vv5) were identified in the VoHV1 genome. Bioinformatic analyses revealed no putative functional domains or motifs of interest in these ORFs.

**Increased SNVs identified in VoHV1 sequence read data.** Tenfold more SNVs were detected in VoHV1 (100 single nucleotide variants [SNVs]) than in PhaHV1 (9 SNVs). All SNVs in PhaHV1 occurred within coding sequences and resulted in nonsynonymous changes. In VoHV1, 86 of the SNVs occurred within a putative coding DNA sequence, and 35 of these were nonsynonymous (Fig. S2). Variant frequencies ranged from 10.2% to 48.0% (mean = 27.0% ± 8.13%) in VoHV1 and 17% to 35% (mean = 29.7% ± 3.6%) in PhaHV1. In VoHV1, the SNVs occurred within 29 annotated ORFs, mostly in core genes, but also in 7 auxiliary (BZLF2 and E3-M4) or novel putative ORFs (V4 to V6, Vv3, and Vv5). In PhaHV1, most SNVs were within the central region of the genome and occurred within five putative ORFs: four core genes and one novel ORF (V3).

**Transcripts mapping to PhaHV1 were identified in koala SRA data sets.** Interrogation of the NCBI Sequence Read Archive (SRA) database was performed to investigate host tissue tropism and to gather viral gene expression information. No VoHV1-specific reads were identified, but PhaHV1-specific transcripts were detected within the koala Transcriptome Sequencing Project (SRA accession number SRP033633) (26), which included transcript data sets from tissues of a female koala with severe chlamydiosis and a male koala attacked by a dog. We detected virus transcripts mostly in the liver and lung, but also in the spleen, of the female koala and mostly in the spleen, bone marrow, and lymph node, but also the liver, from the male koala (Table S2 and Fig. S3). Of these reads, 81% mapped to 35 predicted viral ORFs, with 93.3 to 100% pairwise nucleotide sequence identity with the PhaHV1 reference sequence. Of the 35 ORFs, 4 were shared viral ORFs (V2, V4, V6, V7) and 4 were PhaHV1-specific ORFs (Vp1, Vp3, Vp5, Vp8). The remaining transcripts mapped to five apparently noncoding regions and were mostly centered around ORF49 and ORF50, which are important for the viral lytic cycle (27). Some variants from the PhaHV1 sequence used as a reference were identified, but SNV analysis was not performed because of the very low depth of mapped reads per SNV site (1 to 4 reads), and therefore, the possibility of read sequencing errors could not be excluded. Searches of transcript data sets from other marsupial species (e.g., Tasmanian devil [*Sarcophilus harrisii*], tammar wallaby [*Macropus eugenii*]) did not identify transcripts mapping to the viral genomes (Table S3). Similarly, use of VoHV1 as a query with similar search parameters did not extract virus-specific transcripts from the koala transcriptome data sets, nor did use of the available sequences from other marsupial herpesviruses.

**The putative NTPDase from PhaHV1 hydrolyzes nucleoside tri- and diphosphates *in vitro*.** Recombinant viral NTPDases (vNTPDases) from both PhaHV1 and VoHV1 lacking the predicted TMDs were expressed and purified (Fig. 5) and then tested for NTPDase activity using a capillary electrophoresis (CE)-based enzymatic assay. PhaHV1 NTPDase activity was detected with 6 of the 21 tested substrates: ATP, ADP, GTP, CTP, UTP, and, at a low level, TTP (Table 2). Incubation for 2 h at 37°C was optimal for detection of PhaHV1 NTPDase activity against nucleoside triphosphates. Recombi-

**FIG 3** Legend (Continued)
Predicted viral ACRs are indicated with black boxes. Asterisks indicate conserved residues important for enzymatic function. (B) Neighbor-joining distance tree built using the Jukes-Cantor genetic distance model of amino acid substitution with 1,000 bootstrap replicates. The PhaHV1 and VoHV1 cluster is circled. Mammalian NTPDase clusters are underlined and colored as follows: red, NTPD1 to NTPD3 and NTPD8; blue, NTPD4 and NTPD7; green, NTPD5 and NTPD6. Md, *Monodelphis domestica* (gray short-tailed opossum); Sh, *Sarcophilus harrisii* (Tasmanian devil); Pc, *Phascolarctos cinereus* (koala); H, *Homo sapiens* (human). Refer to Table S4 in the supplemental material for the list of sequences used.

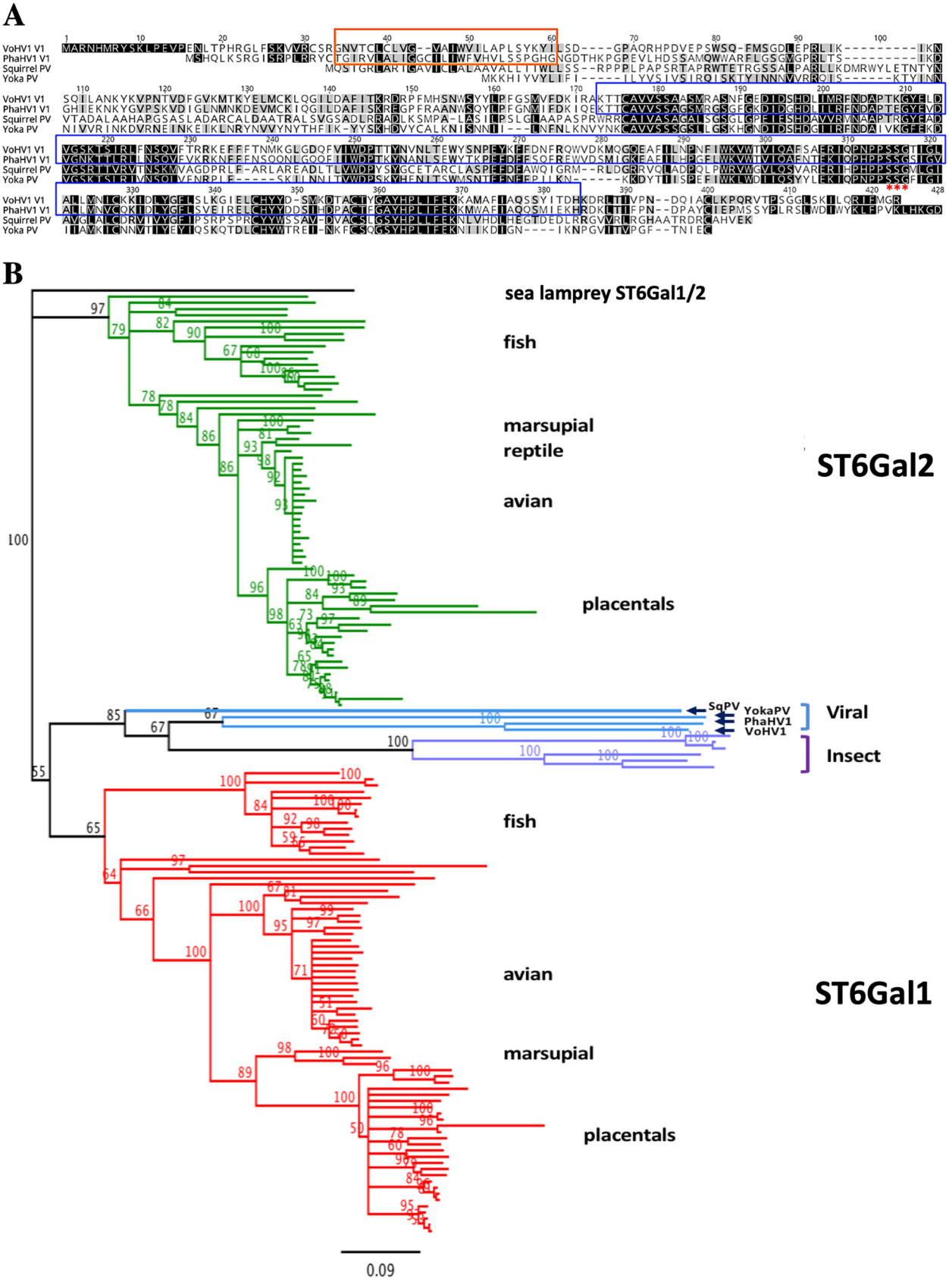


**FIG 4** Sequence structure and phylogenetic comparisons of V1 ORFs from PhaHV1 and VoHV1 with the $\alpha$-2,6-sialyltransferases (ST6Gals) of representative vertebrate, invertebrate, insect, and viral species. (A) ClustalW alignment of virus-encoded ST6Gal polypeptide sequences. Predicted

(Continued on next page)

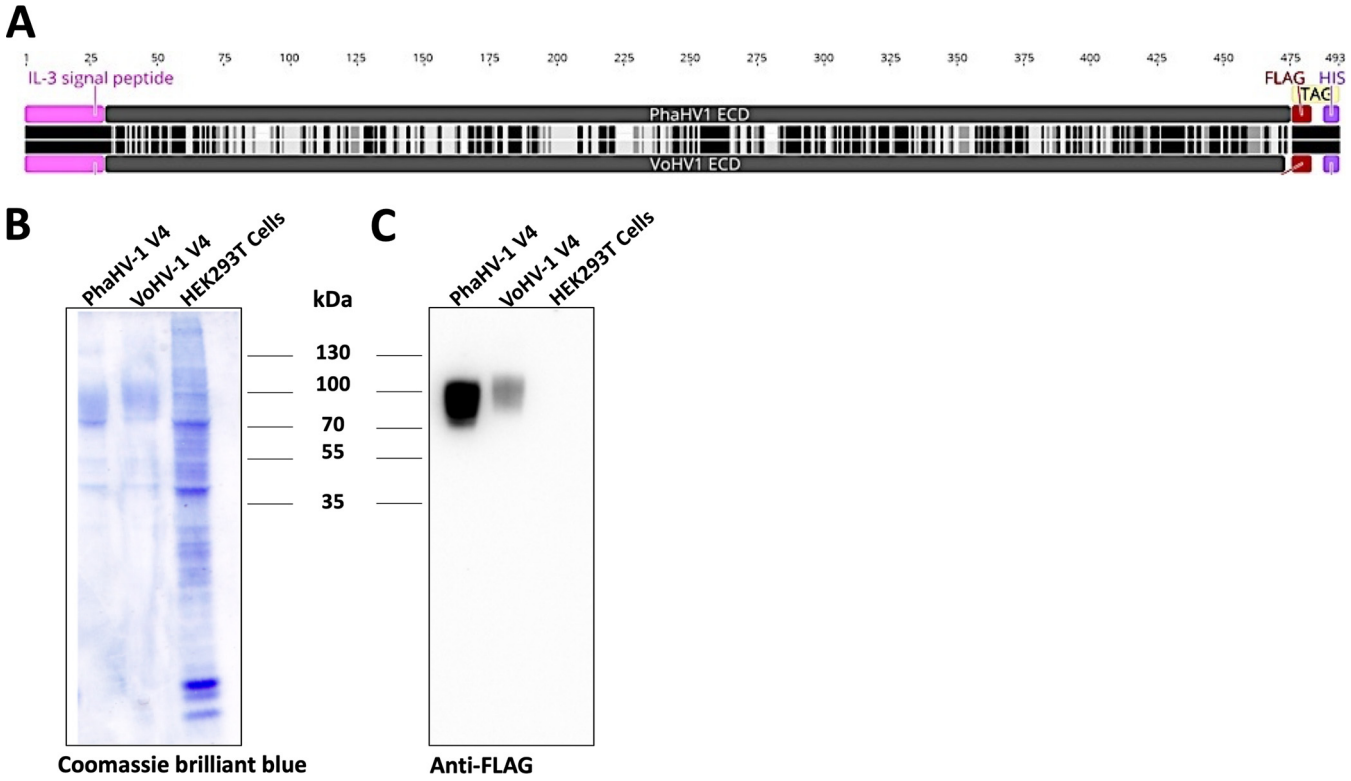


**FIG 5** (A) Design of recombinant expression constructs for viral NTPDase genes from PhaHV1 and VoHV1. The identity of the aligned protein sequences is indicated by an increasingly darker gray scale: light gray, no identity; medium gray, similar; black, identity; dashes, gapped sites. Annotations indicate the extracellular domain (ECD; gray), the IL-3 signal peptide (pink; MVLASSTTSIHTMLLLLLMLFHLGLQASIS), and the C-terminal dual Flag-6×His tag (FLAG-HIS; red and purple, respectively; DYKDDDDKGGGSHHHHHH, where the first and second underlined sequences represent the Flag and His sequences, respectively). (B and C) Purified PhaHV1 and VoHV1 NTPDases stained by Coomassie brilliant blue staining (B) and Western blotting using anti-Flag antibodies (C). HEK293T cell lysate controls are included. The predicted protein sizes are approximately 50 kDa without glycosylation, so the increased sizes of 70 kDa in the reduced fraction may be due to posttranslational modifications. The reduced binding of M2-HRP antibodies to VoHV1 NTPDase may be due to reduced exposure of the Flag epitope region.

nant VoHV1 V4 was tested against nine of the substrates but showed minimal activity (<3% conversion) (Table 2). Other nucleotides, including cyclic mono- and dinucleotides, dinucleotide polyphosphates, nucleotide sugars, and *p*-nitrophenylated nucleotide monophosphates and *p*-nitrophenyl phenylphosphate (*p*-NPPP), were not hydrolyzed by either of the recombinant viral proteins.

Enzyme kinetic analyses were performed on the four nucleoside triphosphates that PhaHV1 was most active against: ATP, GTP, CTP, and UTP. ATP and GTP showed the lowest affinity for the active site (Michaelis-Menten constant [$K_m$] values, 409 $\mu$M and 381 $\mu$M, respectively) compared to that of CTP and UTP ($K_m$ values, 205 $\mu$M and 206 $\mu$M, respectively). Though conversion to products was faster for ATP and GTP than for CTP and UTP, the substrate specificity parameter ($k_{cat}/K_m$) values were similar for all 4 substrates (224 to 300 $M^{-1}\cdot s^{-1}$), suggesting that the relative rate of hydrolysis for each substrate was similar (Fig. 6). The $k_{cat}/K_m$ values for the four substrates were relatively low compared to those for the other ectonucleotidases (28).

**Inhibitor screening, $IC_{50}$ determination, and mechanism of inhibition.** Inhibitor screening utilized a small library of 20 compounds (Table 3) with diverse structures

**FIG 4** Legend (Continued)
PhaHV1 and VoHV1 transmembrane and catalytic domains are outlined in orange and blue boxes, respectively, and substrate-binding sites (SSG) are indicated with red asterisks. The identity of aligned proteins sequences is indicated by an increasingly darker gray scale: light gray, no identity; medium gray, similar; black, identity; dashes, gapped sites. (B) Neighbor-joining distance tree built using the Jukes-Cantor genetic distance model of amino acid substitution with 1,000 bootstrap replicates. The viral cluster is indicated in blue, with the PhaHV1 and VoHV1 branches marked, and the ST6Gal1 and ST6Gal2 clusters are indicated. Refer to Table S5 in the supplemental material for the list of sequences used. PV, poxvirus.

**TABLE 2** Substrates used to test PhaHV1 and VoHV1 recombinant proteins for enzymatic activity and percentage of total nucleotide converted to NMP or NDP products after 2 h of incubation at 37°C, quantified using CE[a]

| | | | PhaHV1 NTPDase | | | VoHV1 NTPDase | | |
|---|---|---|---|---|---|---|---|---|
| Substrate | Concn ($\mu$M) | Assay | Activity detected | % NMP (avg) | % NDP (avg) | Activity detected | % NMP (avg) | % NDP (avg) |
| ATP | 1,000 | CE | Yes | 10.5 | 1.0 | Yes | 0.3 | 2.4 |
| ADP | 1,000 | CE | Yes | 21.5 | | Yes | 1.9 | |
| AMP | 1,000 | MG | No | | | No | | |
| GTP | 1,000 | CE | Yes | 26.5 | −2.0 | Yes | 0.6 | −0.9 |
| CTP | 1,000 | CE | Yes | 15.5 | 1.5 | Yes | 0.6 | 2.9 |
| TTP | 1,000 | CE | Yes | 2.0 | 0.0 | Yes | 0.4 | 1.6 |
| UTP | 1,000 | CE | Yes | 11.0 | 0.5 | Yes | 0.3 | 1.0 |
| 2′,3′-cAMP | 1,000 | CE | No | | | — | | |
| 3′,5′-cAMP | 1,000 | CE | No | | | — | | |
| 3′,3′-c-di-IMP | 200 | CE | No | | | — | | |
| 3′,3′-c-di-GMP | 200 | CE | No | | | — | | |
| 2′,5′-c-di-GMP | 200 | CE | No | | | — | | |
| 2′,3′-cGAMP | 200 | CE | No | | | — | | |
| 3′,3′-cGAMP | 200 | CE | No | | | — | | |
| AP3A | 200 | CE | No | | | — | | |
| AP4A | 200 | CE | No | | | — | | |
| UDP-glucose | 1,000 | CE | No | | | — | | |
| NAD | 1,000 | CE | No | | | — | | |
| *p*-Nph-5′-TMP | 1,000 | *p*-NP | No | | | No | | |
| *p*-Nph-5′-AMP | 1,000 | *p*-NP | No | | | No | | |
| *p*-NPPP | 1,000 | *p*-NP | No | | | No | | |

[a]NMP, nucleoside monophosphate; NDP, nucleoside diphosphate; MG, malachite green; CE, capillary electrophoresis; —, not tested; UDP-glucose, uracil diphosphate glucose; cAMP, cyclic AMP; c-di-IMP, cyclic di-inosine monophosphate; c-di-GMP, cyclic diguanosine monophosphate; cGAMP, cyclic guanosine AMP; AP3A, diadenosine triphosphate; AP4A, diadenosine tetraphosphate; *p*-Nph-5′-TMP, *p*-nitrophenyl 5′- dTMP; *p*-Nph-5′-AMP, *p*-nitrophenyl 5′-AMP; *p*-NPPP, *p*-nitrophenyl phenylphosphate.

known to be potent inhibitors of NTPDases from eutherian mammals (specifically, human and rat) (29). The ability of compounds to inhibit the hydrolysis of ATP to AMP by the PhaHV1 enzyme was tested in a CE-based assay and a malachite green (MG) phosphate assay (Fig. 7). Both assays yielded comparable results. Nine compounds inhibited the PhaHV1 enzyme activity by ≥70%, and two compounds, compound 4 (PV4, PSB-POM141, $K_6H_2[TiW_{11}CoO_{40}]\cdot 13H_2O$) and compound 9 ($Na_{14}[P_5W_{30}O_{110}]\cdot 30H_2O$), completely inhibited enzymatic activity at 10 $\mu$M. A concentration-inhibition 50% inhibitory concentration ($IC_{50}$) assay demonstrated that compound 9 was more potent than compound 4 ($IC_{50}$s, 0.169 ± 0.005 $\mu$M and 0.784 ± 0.176 $\mu$M, respectively) (Fig. 8). As both compounds typically acted via a similar mechanism on other NTPDases, the mechanism of inhibition was determined experimentally only for compound 9. A Hanes-Woolf plot analysis showed that it acted as a noncompetitive inhibitor of the PhaHV1 enzyme (Fig. 8) by crossing all lines at the *x* axis, which suggested that the $K_i$ values of compound 9 (and compound 4) are approximately equivalent to their $IC_{50}$ values.

## DISCUSSION

The PhaHV1 and VoHV1 genomes are the first marsupial gammaherpesvirus genomes to be sequenced. Although a macropod alphaherpesvirus (MaHV1) genome was published in 2016 (19), gammaherpesviruses are of particular interest because of their typically restricted host and tissue range and apparently greater variation between viral species (30, 31). It is consistent with the evolutionary history of marsupials and their early divergence from eutherian mammals (1, 2) to find that gammaherpesviruses that infect and that have probably coevolved with marsupials formed an isolated branch outside the existing gammaherpesvirus genera.

The SNV analysis identified a relatively high number of SNVs in the VoHV1 sequence data set, with read frequencies of up to 48%, indicating that there was probably a mixed population of VoHV1s within the original sample. Similarly, SNV analysis of the PhaHV1 read data indicated that the source animal was also likely the host to multiple virus variants, although the lower frequency of SNVs and their nonsynonymous nature

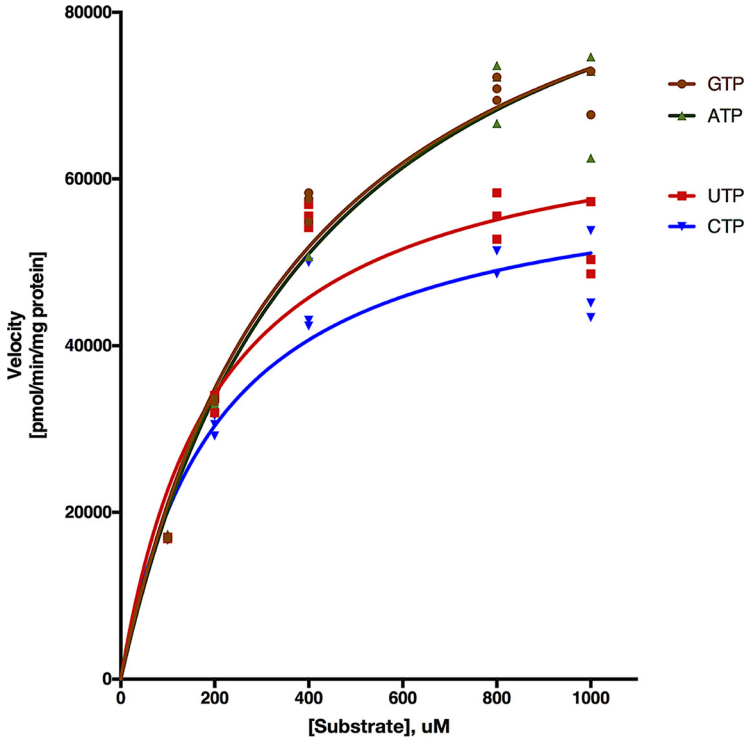


| Substrate | $K_m$ | | $V_{max}$ | | $k_{cat}$ | | $k_{cat}/K_m$ ($M^{-1}.s^{-1}$) |
|---|---|---|---|---|---|---|---|
| | $\mu$M | SD | $\mu$M / min | SD | $10^{-3}.s^{-1}$ | SD | |
| ATP | 409.4 | 61.8 | 5.0 | 0.3 | 91.9 | 5.8 | 224.5 |
| GTP | 381.4 | 55.4 | 4.9 | 0.3 | 90.1 | 5.3 | 236.3 |
| CTP | 205.7 | 40.6 | 3.0 | 0.2 | 54.9 | 3.4 | 266.6 |
| UTP | 205.2 | 52.5 | 3.3 | 0.3 | 61.6 | 5.0 | 300.4 |

**FIG 6** Michaelis-Menten plots for PhaHV1 NTPDase activity with GTP, ATP, UTP, or CTP as the substrate and the corresponding kinetic values for each substrate. Nonlinear regression was performed using GraphPad Prism software.

may suggest that culture of this koala virus on wombat cells placed it under a higher selective pressure, resulting in a restricted SNV profile, or bottlenecking (32, 33). Infection with multiple strains of the same gammaherpesvirus species has been documented in other hosts (34–38). Interrogation of the koala transcriptomic data sets detected PhaHV1 in two animals and in multiple tissues. Some of these sites of viral replication (spleen and liver) were already known (11), but others (bone marrow, lung, lymph node) had not been reported previously.

The genomes of both viruses encoded putative NTPDase and ST6Gal1-like proteins. The presence of genes encoding these enzymes has not been reported previously in a herpesvirus, and an NTPDase gene has never been reported in any virus to date. Their positional and sequence homology, as well as phylogenetic comparisons to homologs in vertebrates and pathogens, indicated that they were likely acquired in a single event, prior to their viral evolutionary divergence and possibly prior to the speciation of koalas and wombats, which is estimated to have occurred 30 million to 40 million years ago (39). While it is likely that these genes were acquired from a common ancestor of koalas and wombats, the vNTPDases and viral ST6Gal1 shared only 35% to 37% pairwise amino acid sequence identity with those of contemporary mammals.

Members of the ST6Gal family of enzymes are broadly expressed across most taxonomic lineages, including vertebrates, invertebrates, and insects. They are typically localized to the Golgi apparatus, where they sialylate galactose-containing glycosylated products. STGal1s are essential for regulating the production of multiple T and B lymphocyte cell surface differentiation antigens, CD75, HB-6, and CD76 (40), as well as regulating macrophage apoptosis (41). To our knowledge, no ST6Gal homologs have

**TABLE 3** NTPDase inhibitor compounds tested in PhaHV1 NTPDase inhibition studies

| Inhibitor no. | Inhibitor | Formula | Mol wt (Da) |
|---|---|---|---|
| 1 | PV1 | $Na_6(H_2W_{12}O_{40})\cdot 21H_2O$ | 3,366 |
| 2 | PV2 | $H_3(PW_{12}O_{40})\cdot H_2O$ | 2,880 |
| 3 | PV3 | $K_7(Ti_2W_{10}PO_{40})\cdot 8H_2O$ | 3,023 |
| 4 | PV4 | $K_6H_2(TiW_{11}CoO_{40})\cdot 13H_2O$ | 3,240 |
| 5 | PV5 | $K_{10}[Co4(H_2O)2(PW_9O_{34})2]\cdot 22H_2O$ | 5,518 |
| 6 | PV6 | $(NH_4)_{18}(NaSb_9W_{21}O_{86})\cdot 14H_2O$ | 6,932 |
| 7 | $NaPW_{12}$ | $Na_3(PW_{12}O_{40})\cdot 7H_2O$ | 3,074 |
| 8 | $NaP_6W_{18}$ | $Na_{20}(P_6W_{18}O_{79})\cdot 37H_2O$ | 5,888 |
| 9 | $NaP_5W_{30}$ | $Na_1(NaP_5W_{30}O_{110})\cdot 30H_2O$ | 8,320 |
| 10 | Reactive blue 2 | $C_{29}H_{20}ClN_7Na_3O_{11}S_3$ | 774 |
| 11 | KB1 | $K_4[(Re_6S_8)(OH)_6]\cdot 8H_2O$ | 1,776 |
| 12 | KB2 | $K_4[(Re_6Se_8)(OH)_6]\cdot 8H_2O$ | 2,151 |
| 13 | KB3 | $K_4[(Re_6S_8)(CH_3COO)_6]\cdot 8H_2O$ | 2,028 |
| 14 | KB4 | $K_4[(Re_6S_8)(HCOO)_6]\cdot 3H_2O$ | 1,854 |
| 15 | Le135 | $C_{29}H_{30}N_2O_2$ | 439 |
| 16 | Resveratrol | $C_{14}H_{12}O_3$ | 228 |
| 17 | Quercetin | $C_{15}H_{10}O_7$ | 302 |
| 18 | Suramin | $C_{51}H_{40}N_6O_{23}S_6$ | 1,297 |
| 19 | Methotrexate | $C_{20}H_{22}N_8O_5$ | 454 |
| 20 | IBMX[a] | $C_{10}H_{14}N_4O_2$ | 222 |

[a]IBMX, 3-isobutyl-1-methylxanthine.

been reported in prokaryotes or parasites to date. Although unusual in viruses, the ST6Gal homolog encoded by V1 is among a small number of viral sialyltransferases that have previously been identified in only three poxviruses. These are an ST6Gal in Yoka poxvirus (a 1972 isolate from a mosquito pool) and squirrel poxvirus (a cause of lethal outbreaks of disease in Eurasian red squirrels [*Sciurus vulgaris*]), with which V1 appears to form a clade, and an ST3Gal ($\alpha$-2,3-sialyltransferase) encoded by the genome of myxoma virus (the cause of lethal disease in European rabbits [*Oryctolagus cuniculus*]) (24, 42, 43). In myxoma virus, the ST3Gal homolog has been identified to be a virulence determinant, and its absence enhances both inflammatory cell migration to the site of infection and the neutralizing antibody response to infection (42, 44). The role of virus-encoded ST6Gal homologs has not been investigated, so it is unknown whether it would have a similar effect and function during viral infection.

The NTPDase family of enzymes is commonly distributed across animal species and is present in many pathogenic protists, although the role of these enzymes in these organisms is poorly defined (45). Many NTPDases are membrane bound, and four of the eight mammalian subtypes are cell surface localized with an extracellular active site (46). In mammals, these cell surface-localized NTPDases play key roles in thromboregulation, inflammation, and immune suppression by affecting the extracellular concentration of nucleoside tri- and diphosphates, with subsequent effects on the purinergic receptors involved in these processes (46, 47). In humans, NTPDases are a therapeutic target for both genetic and infectious diseases (29, 47–50) and so may also have potential as an antiviral target.

Initial sequence analysis of the PhaHV1 NTPDase homolog revealed the presence of all gene features that are reportedly important for enzyme activity (51). Purification and enzymatic characterization of recombinant PhaHV1 NTPDase demonstrated hydrolysis of nucleoside tri- and diphosphates in the presence of divalent cations, but no other type of nucleotidase activity was detected, as is typical for the NTPDase family. The affinity of PhaHV1 NTPDase for the nucleoside triphosphates (NTPs) tested was lower than that of mammalian (human and rat) NTPDases 1 to 3 ($K_m$ for vNTPDase = 200 to 400 $\mu$M; $K_m$ for human NTPDases 1 to 3 = 10 to 200 $\mu$M) (51) but was still within the same order of magnitude, suggesting that the enzyme is likely active at the physiological concentrations at which NTPs can be found in mammalian hosts.

The role of V4 during PhaHV1 infection is unknown, though herpesviruses are most active (and cause disease) when hosts are stressed or immunosuppressed (5). Extracellular ATP is a danger signal for the host, and activation of purinergic receptors by ATP

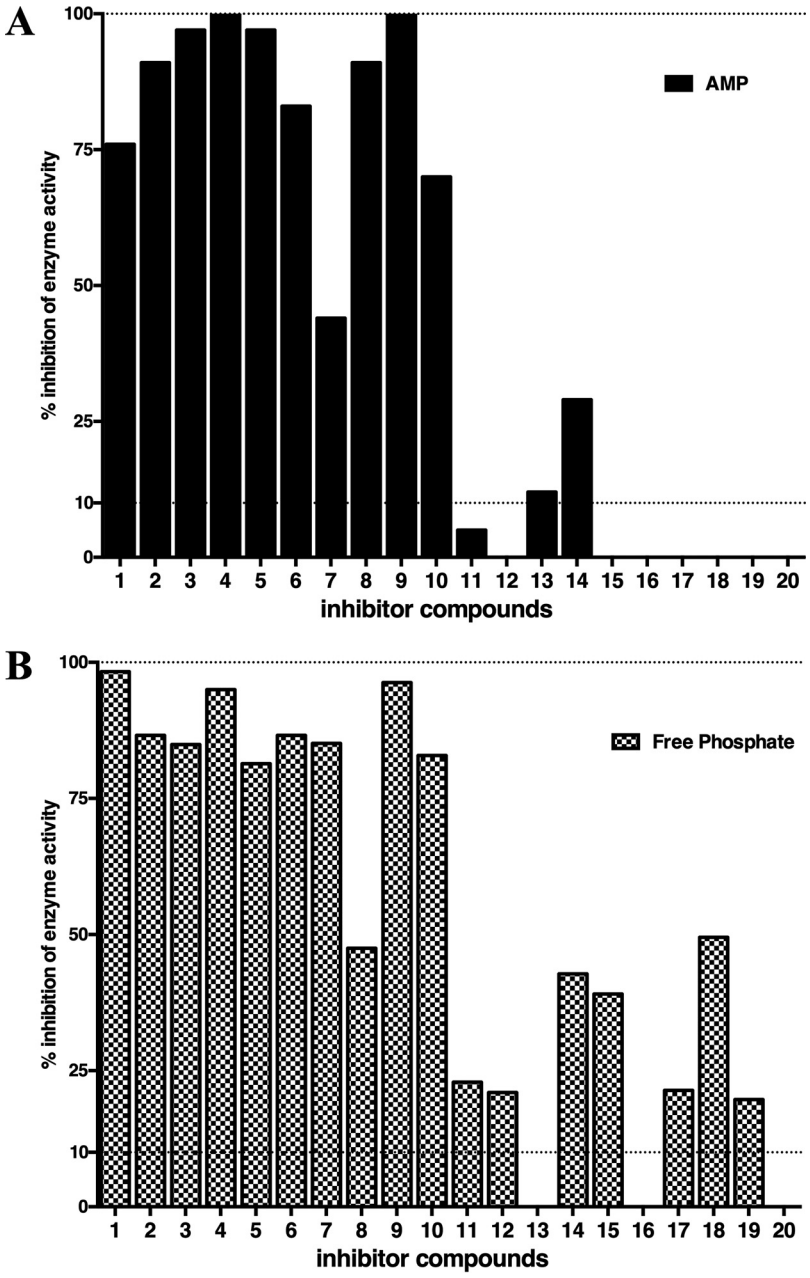


**FIG 7** Inhibitor screening results of PhaHV1 NTPDase activity using a panel of 20 known inhibitors of NTPDases from placental mammals. (A) The ability of these compounds to inhibit hydrolysis of ATP to AMP by the PhaHV1 enzyme was tested using a CE-based assay. (B) Individual members of the compound library were also tested with the malachite green method, used to measure $P_i$ production. Compounds were screened at 10 $\mu$M, and the percent inhibition of enzymatic activity was calculated. The detection of NTPDase inhibitors using this method was comparable to that using CE-based assays. Refer to Table 3 for the list of compounds used.

is a key component of the inflammatory process (52). Expression of the enzyme on the surface of the host cell may reduce the inflammatory response by lowering ATP (and ADP) concentrations and reducing activation of proinflammatory P2 receptors, leading to increased concentrations of AMP. This is further converted to anti-inflammatory and immunosuppressive adenosine by another mammalian ectonucleotidase, CD73 (or ecto-5′-nucleotidase), with the effect of redirecting the immune response toward the P1 (adenosine) receptor pathways, resulting in local immunosuppression through altered cytokine expression profiles or inhibition of apoptotic cellular pathways (51).

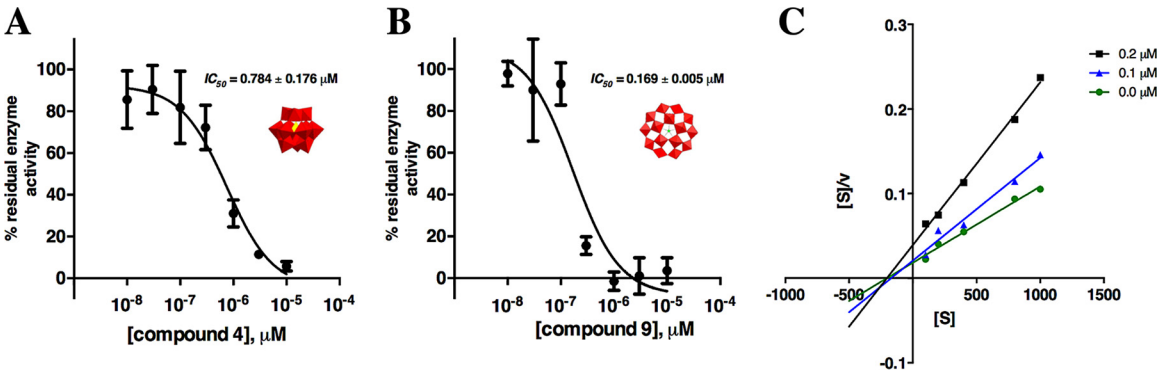


**FIG 8** Concentration-inhibition curves for polyoxometalate compounds 4 [$(TiW_{11}CoO_{40})^{8-}$, PV4, or PSB-POM141] (A) and 9 [$(NaP_5W_{30}O_{110})^{14-}$ or $NaP_5W_{30}$] (B) against PhaHV1 NTPDase. (C) Hanes-Woolf plot of vNTPDase inhibition by compound 9, indicating that it acts as a noncompetitive inhibitor of the viral enzyme. [S], concentration of ATP substrate (in micromolar); v, velocity of reaction (in nanomoles per minute per milligram of protein); $IC_{50}$, the concentration of an inhibitor showing 50% residual enzyme activity. A schematic representation of the structure of each compound, adapted from reference 29, is shown in red.

Our results show that PhaHV1 NTPDase readily hydrolyzes ADP. Hydrolysis of ATP to only ADP promotes platelet aggregation, which is one role of NTPDase2 (53), whereas ongoing hydrolysis to AMP results in inhibition of platelet aggregation (54), which may be advantageous during viral infection.

Further biochemical analysis is needed to determine if the VoHV1 V4 encodes a functional NTPDase or another biologically relevant active enzyme. An incomplete ACR4 in VoHV1 V4 may explain the negligible activity detected against the NTP and nucleoside diphosphate (NDP) substrates tested, though other contributing factors could be the removal of the TMDs (which can affect the activity of mammalian NTPDases) or a lack of the preferred divalent cation (only $Mg^{2+}$ and $Ca^{2+}$, two commonly preferred cations for NTPDases, were tested) (55). The presence of a second ACR3 could also have resulted in an altered functional state. For example, this protein may play a different (nonnucleotidase-like) role during VoHV1 infection. Other NTPDases have been identified in the genomes of bacteria (e.g., *Legionella*), fungi (e.g., *Candida*, *Cryptococcus*), and parasites (e.g., *Plasmodium*, *Leishmania*, and *Schistosoma*). While in some cases they have been identified as a virulence factor, e.g., in *Legionella pneumophila* (50), for most of these pathogens the precise role or importance of their encoded NTPDases has not been described. Although this is the first NTPDase encoded by a virus, it is not the first example of the viral appropriation of NTPDases. In human immunodeficiency virus infection there is an increase in NTPDase1 (CD39) expression, and functional host NTPDase1 can be found embedded in the viral envelope (56, 57). Further localization and functional enzymatic studies, as well as targeted transcriptomic or proteomic studies, may help identify what purpose these viral NTPDases have during infection.

Our understanding of the role of herpesviruses in marsupial health is still in its infancy. A 2015 study of marsupials in the Australian state of Victoria detected herpesviruses in 33.3% of koalas and 45.5% of wombats. Herpesvirus infections were significantly associated with both poor body condition in wombats and coinfection with *Chlamydia pecorum* in koalas, but the direct clinical relevance of these herpesviruses remains undetermined (13). This is consistent with studies of gammaherpesviruses in other species, which indicate that their clinical effects can be insidious and difficult to evaluate, particularly in nonlaboratory animal populations (6, 58–60). Currently, there are no treatments for herpesvirus-induced diseases in any marsupial species, but the therapeutic potential of inhibitors that prevent the degradation of extracellular nucleotides by host- and/or pathogen-derived enzymes is of interest in treating human diseases (29, 47–50). This study identified 9 compounds capable of inhibiting viral NTPDase activity; however, their effect on an active viral infection remains to be determined. As the inhibitors selected for this

study are known to be potent inhibitors of mammalian (eutherian) NTPDases, it is likely that they inhibit host enzymes and virus-expressed homologs. Although this may have possible benefits in alleviation of virus-induced immunosuppression, evidence of a direct interaction with viral NTPDase would be difficult to demonstrate *in vivo*. The future identification of inhibitors that are specifically active against the viral (rather than host) enzymes offers a potential target for controlling herpesvirus infection in koalas and wombats.

## MATERIALS AND METHODS

**Virus propagation and genome sequencing and assembly.** The PhaHV1 and VoHV1 isolates originated from an oropharyngeal swab specimen from a koala and a nasal swab specimen from a bare-nosed wombat, respectively, and were cultured in wombat joey primary kidney cells (13). Approval for swab collection was granted by the Animal Ethics Committee for the Faculty of Veterinary Science, The University of Melbourne (Animal Ethics ID 1112058.1). Herpesvirus nucleocapsid DNA was sequenced, using Illumina MiSeq paired-end chemistry, and genomes were assembled as described previously (19), with minor modifications. Specifically, conserved gammaherpesvirus ORF arrangements (61) were used as a guide to construct the final genomic structures. Regions of unresolved ambiguity, primarily due to tandemly repeating sequences, were annotated as such.

**Genome annotation and single nucleotide variant analysis.** Prediction of ORFs using a Glimmer3 system was restricted to core genomic regions of low ambiguity and to ORFs larger than 250 bp. ORF annotation was performed by searching against the NCBI nonredundant protein and nucleotide databases with the BLASTX and BLASTN programs, respectively (62, 63). Predicted ORFs of unknown function were annotated as hypothetical proteins, and their sequences were analyzed using the PFAM database and the Conserved Domain Database (CDD) to predict their putative function. Other sequence analysis algorithms used were SignalP to identify putative signal peptides, TMHMM (64, 65) to identify transmembrane domains, and Phobius, a combined transmembrane and signal peptide prediction tool for cellular localization predictions. Similarity searches at the level of secondary and tertiary protein structure were performed using the I-TASSER server (66). Threshold cutoff values of $>1$ for the normalized Z-score, a root mean square deviation (RMSD) of $<3.0$, and a template modeling (TM) score of $>0.7$ for these were considered significant and used to identify structural homologs. The nomenclature of common gene annotations followed the gammaherpesvirus naming convention (21, 67–69), while PhaHV1/VoHV1 shared hypothetical/novel ORFs were prefixed with V (*Vombatiformes*) and virus-specific unique ORFs were prefixed with Vp (PhaHV1) or Vv (VoHV1).

Single nucleotide variant analysis was performed with a minimum variant frequency threshold of 0.10, a maximum variant *P* value of $10^{-6}$ (determined using the approximate *P* value calculation method), and the plug-in default setting of a minimum-strand-bias *P* value of $10^{-5}$ with a threshold bias of 65%. Regions of low sequence confidence, specifically, unresolved sites with complex sequence repeats, were excluded from variant analysis to reduce the incidence of false-positive results. Variant analyses were performed using the software package Geneious (version 9.1.5).

***In vivo* ORF transcript detection.** Interrogation of public transcript data sets was performed using the Sequence Read Archive nucleotide BLAST (SRA-BLAST) function in the NCBI website (https://www.ncbi.nlm.nih.gov/sra). We used the assembled viral genomes as the query to search all marsupial SRA experimental gene expression data sets (see Table S3 in the supplemental material). Searches were restricted to highly similar sequence settings, using MegaBLAST conditions, in order to exclude non-virus-specific reads.

**Phylogenetic analysis of *Vombatiformes* herpesviruses.** Alignments of the assembled genome sequences of PhaHV1 and VoHV1 (Fig. 1) were prepared using the Multiple Alignment with Fast Fourier Transformation (MAFFT; version 7) plug-in in Geneious (version 6.1.8) software (70). The sequences of regions of high diversity, specifically, the sequence termini, were manually adjusted to obtain a better alignment. Phylogenetic analyses with representative sequences of the *Alpha-*, *Beta-*, and *Gammaherpesvirinae* were performed using the most conserved herpesvirus genes (Fig. 2): DPOL (ORF9) and gB (ORF8). The sequences of the encoded polypeptides were aligned using the MAFFT plug-in, and the alignments were refined using the ClustalW program. Alignment columns containing gaps were removed from all sequences prior to further analysis. Trees were built using maximum likelihood with the Jones-Taylor-Thornton substitution model with 100 bootstrap replicates. Phylogenetic analyses were performed using selected viral ORFs (V1 and V4) that included homologs from representative eukaryotic and prokaryotic taxa. Neighbor-joining distance trees were built using the Jukes-Cantor distance model with 1,000 bootstrap replicates. These polypeptide sequences were aligned as described above for the core ORFs, and phylogenetic alignments were restricted to concatenated conserved ORF regions. The sequences used in all analyses can be found listed in Tables S1, S4, and S5.

**Generation of recombinant viral NTPDases.** Viral NTPDase-like amino acid sequences were evaluated for protein features required for enzymatic activity, including ACRs and conserved cysteine residues (23). A codon-optimized sequence of the predicted extracellular domains (ECD) containing the five putative ACRs was cloned into pCAGGS_MCS, a mammalian cell expression vector (Fig. 5A; GenScript Biotech, China). The predicted native signal sequence was replaced by an interleukin-3 (IL-3) signal sequence to promote protein secretion and C-terminal Flag (DYKDDDDK) and His purification tags. Suspension-adapted cultures of FreeStyle-293 cells (Life Technologies) were grown in Freestyle 293 expression medium (Life Technologies) supplemented with GlutaMAX-I supplement. Scale-up transient

transfection was performed on 1-liter cultures of FreeStyle-293 cells ($2 \times 10^6$ per ml) in a shake flask using linear polyethyleneimine (PEI; Polysciences Inc.) according to a published protocol (71). The cultures were harvested after cell viability reached ~50% (7 to 11 days), clarified by centrifugation, and filtered. Soluble, recombinant viral NTPDases were purified by anti-Flag immunoaffinity chromatography followed by size exclusion chromatography through a Superdex S200 column (GE Healthcare) as previously described (72). Final protein elutions were performed using Tris-buffered saline (5 mM Tris-Cl, pH 7.5, 150 mM NaCl). Eluates were concentrated using Amicon Ultra-15 centrifugal filter units (Merck Millipore), aliquoted, and stored at −70°C until use. Fractions of each protein and an HEK293T cell lysate control were separated on a 4 to 15% mini-Protean TGX precast protein gel (Bio-Rad) as previously described (73) under denaturing conditions. The proteins were transferred to a polyvinylidene difluoride membrane and blocked in phosphate-buffered saline (PBS) containing 0.05% Tween 20 (PBS-T) and 5% (wt/vol) skim milk powder for 60 min at 37°C, the membrane was then incubated with M2-horseradish peroxidase (HRP) antibodies detecting the Flag tag, and binding was detected using a ClarityWestern enhanced chemiluminescence blotting substrate (Bio-Rad),

**Substrate screening.** PhaHV1 recombinant V4 was screened against the 21 substrates in Table 2 (in duplicate) by CE, an MG phosphate assay, or a *p*-nitrophenolate (*p*-NP)-based assay (28). The assay buffer for the CE system contained $Ca^{2+}$ (without $Mg^{2+}$), as $Ca^{2+}$ yielded the highest activity in this system. The concentrations of the substrates were 0.2 or 1.0 mM with 2.4 $\mu$g of each vNTPDase in reaction buffer (10 mM HEPES, 2 mM $CaCl_2$, pH 7.4) and 10% (vol/vol) dimethyl sulfoxide (DMSO). The reaction mixtures were incubated for 1 and 2 h at 37°C and then for 3 min at 90°C to stop the reactions. No-enzyme (substrate-only) controls were included for each substrate, and 20 $\mu$M monophosphates (AMP, GMP, UMP, CMP, TMP) were used as standards. The reaction mixtures were diluted 1 in 3 (0.2 mM substrate reaction mixtures) or 1 in 10 (1.0 mM substrate reaction mixtures) in reaction buffer prior to CE to prevent overloading the instrument. CE analyses were carried out using a P/ACE MDQ capillary electrophoresis system (Beckman Instruments, USA), and data collection and peak area analysis were performed using the P/ACE MDQ software 32 KARAT (Beckman Coulter, USA). The electrophoretic separations were performed in a 40-cm polyacrylamide-coated capillary (CS-Chromatography, Langerwehe, Germany) with electrokinetic injections at a voltage of −6 kV for 30 s and separations at a voltage of −15 kV using 100 mM phosphate buffer (pH 6.5). Analytes were detected using direct UV absorbance at 260 nm with a diode array detection system. The hydrolysis of AMP was investigated using the MG assay, and enzymatic assay conditions were as described above for the CE-based analysis, but the detection of released inorganic phosphate was performed using a PHERAstar plate reader (BMG Labtech GmbH, Ortenberg, Germany) (74).

A series of artificial substrates, including *p*-nitrophenyl-5′-dTMP (*p*-Nph-5′-TMP), *p*-nitrophenyl-5′-AMP (*p*-Nph-5′-AMP), and *p*-nitrophenyl phenylphosphate (*p*-NPPP), was investigated using the *p*-nitrophenolate (*p*-NP)-based assay (28). Briefly, 2.4 $\mu$g of each vNTPDase was incubated at 37°C for 2 h with each substrate (1 mM) in reaction buffer and 10% (vol/vol) DMSO in triplicate. The reactions were stopped using 20 $\mu$l of 1.0 M NaOH, and the release of *p*-NP was measured at 400 nm using a PHERAstar plate reader, with human NPP1 included as a positive reaction control and 20 $\mu$M *p*-NP included as a standard.

**Enzyme kinetic analysis to determine substrate preference.** Detailed enzyme kinetic analysis was performed for PhaHV1 NTPDase. The Michaelis-Menten constant ($K_m$), maximal velocity ($V_{max}$), turnover number ($k_{cat}$), and substrate specificity parameter ($k_{cat}/K_m$) values were determined for the nucleoside triphosphate substrates ATP, GTP, CTP, and UTP. Briefly, 2.4 $\mu$g of vNTPDase was incubated for 2 h at 37°C with substrates at concentrations of 0.1, 0.2, 0.4, 0.8, 1.0, 2.0, 4.0, or 8.0 mM in reaction buffer, in triplicate. CE conditions were as described above with 8 to 10 min of separation at −15 kV. Data were analyzed using GraphPad Prism (version 6.0) software.

**Inhibitor screening, $IC_{50}$ determination, and mechanism of inhibition.** Twenty compounds known to act as potent inhibitors of mammalian NTPDases were tested for their ability to inhibit the PhaHV1 NTPDase-catalyzed conversion of ATP to ADP and AMP. Briefly, 2.4 $\mu$g of vNTPDase and 400 $\mu$M ATP were incubated for 2 h at 37°C with 10 $\mu$M each compound (dissolved in 10% DMSO). Inhibitor-free controls (enzyme plus substrate only) were included in triplicate as blanks, and inhibition values were determined relative to blank conversion values. Reaction samples were diluted 1 in 4 in reaction buffer and analyzed using CE and MG assays. CE conditions were as described above, with 14 to 16 min of separation at −10 kV, and the results of the MG phosphate assays were measured on a PHERAstar plate reader (BMG Labtech) at 623 nm (74).

Concentration-inhibition curves were performed by incubating 2.4 $\mu$g of vNTPDase with 400 $\mu$M ATP for 2 h at 37°C with inhibitor at a concentration of 0.01, 0.03, 0.1, 0.3, 1.0, 3.0, or 10.0 mM in reaction buffer with 10% DMSO in triplicate. No-enzyme (0.01 $\mu$M inhibitor and 400 $\mu$M ATP only), no-inhibitor, and buffer-only samples were included as reaction controls. Phosphate concentrations were measured using MG phosphate assays, as described above (74). Percent residual protein activity values were calculated relative to the activity for the inhibitor-free controls.

The mechanism of inhibition was determined by testing the inhibitors at 0, 0.1, and 0.2 $\mu$M (in 10% DMSO) with substrate (ATP) at 0.1, 0.2, 0.4, 0.8, or 1 mM and 2.4 $\mu$g of vNTPDase protein (37°C, 2 h, in reaction buffer). The phosphate released was measured by the MG assay, and the type of inhibition was evaluated graphically from a Hanes-Woolf plot using GraphPad Prism (version 6.0) software (74).

**Data availability.** The sequences were deposited in GenBank under accession numbers MG452721 and MG452722. Raw read data sets were submitted to the NCBI Sequence Read Archive (SRA) under BioProject number PRJNA477676.

## SUPPLEMENTAL MATERIAL

Supplemental material for this article may be found at https://doi.org/10.1128/JVI.01404-18.

**SUPPLEMENTAL FILE 1**, PDF file, 5.5 MB.

## ACKNOWLEDGMENTS

We thank Zoos Victoria and Wildlife Health Surveillance Victoria, particularly Pam Whiteley, for assistance with sample collection. Special thanks go to Nino Ficorilli for his valuable help with the wombat kidney cells and to Cynthia Brown for her excellent technical assistance.

Paola K. Vaz was supported by the Victoria state government through a 2016 Victoria Fellowship, and further funding for this study was provided by the Australian government through the National Collaborative Research Infrastructure Strategy.

P.K.V. performed the viral DNA sequence analysis, designed the expression plasmids, and performed the enzymatic characterization experiments in the laboratory of C.E.M. T.E.A., L.P., and G.L. provided NTPDase construct design advice and performed the large-scale viral NTPDase purification. S.-Y.L. and C.E.M. provided the reagents, facilities, and guidance for the viral NTPDase substrate and inhibitor screening experiments. F.M.S. provided NTPDase characterization advice. K.S. provided the viral isolates and performed the VoHV1 DNA purification. C.A.H., G.F.B., and J.M.D. contributed to the design of the project and provided advice on data analysis. All coauthors contributed to the editing and drafting of the manuscript.

## REFERENCES

1. Bininda-Emonds ORP, Cardillo M, Jones KE, MacPhee RDE, Beck RMD, Grenyer R, Price SA, Vos RA, Gittleman JL, Purvis A. 2007. The delayed rise of present-day mammals. Nature 446:507–512. https://doi.org/10.1038/nature05634.
2. Clemens WA. 1970. Mesozoic mammalian evolution. Annu Rev Ecol Syst 1:357–390. https://doi.org/10.1146/annurev.es.01.110170.002041.
3. McGeoch DJ, Dolan A, Ralph AC. 2000. Toward a comprehensive phylogeny for mammalian and avian herpesviruses. J Virol 74:10401–10406. https://doi.org/10.1128/JVI.74.22.10401-10406.2000.
4. McCarthy K, Tosolini FA. 1975. Hazards from simian herpes viruses: reactivation of skin lesions with virus shedding. Lancet i:649–650. https://doi.org/10.1016/S0140-6736(75)91756-0.
5. Pellet P, Roizman B. 2013. Herpesviridae. *In* Knipe D, Howley PM, Cohen JI, Griffin DE, Lamb RA, Martin MA, Racaniello VR, Roizman B (ed), Fields virology, vol 2, 6th ed. Lippincott Williams & Wilkins, Philadelphia, PA.
6. Alibek K, Baiken Y, Kakpenova A, Mussabekova A, Zhussupbekova S, Akan M, Sultankulov B. 2014. Implication of human herpesviruses in oncogenesis through immune evasion and supression. Infect Agents Cancer 9:3. https://doi.org/10.1186/1750-9378-9-3.
7. Finnie EP, Littlejohns IR, Acland HM. 1976. Letter: mortalities in parma wallabies (*Macropus parma*) associated with probable herpesvirus. Aust Vet J 52:294. https://doi.org/10.1111/j.1751-0813.1976.tb00123.x.
8. Callinan RB, Kefford B. 1981. Mortalities associated with herpesvirus infection in captive macropods. J Wildl Dis 17:311–317. https://doi.org/10.7589/0090-3558-17.2.311.
9. Wilks CR, Kefford B, Callinan RB. 1981. Herpesvirus as a cause of fatal disease in Australian wallabies. J Comp Pathol 91:461–465. https://doi.org/10.1016/0021-9975(81)90019-0.
10. Vaz P, Whiteley PL, Wilks CR, Browning GF, Gilkerson JR, Ficorilli N, Devlin JM. 2012. Detection of a second novel gammaherpesvirus in a free-ranging koala (*Phascolarctos cinereus*). J Wildl Dis 48:226–229. https://doi.org/10.7589/0090-3558-48.1.226.
11. Vaz P, Whiteley PL, Wilks CR, Duignan PJ, Ficorilli NP, Gilkerson JR, Browning GF, Devlin JM. 2011. Detection of a novel gammaherpesvirus in koalas (*Phascolarctos cinereus*). J Wildl Dis 47:787–791. https://doi.org/10.7589/0090-3558-47.3.787.
12. Vaz PK, Motha J, McCowan C, Ficorilli N, Whiteley PL, Wilks CR, Hartley CA, Gilkerson JR, Browning GF, Devlin JM. 2013. Isolation and characterization of a novel herpesvirus from a free-ranging eastern grey kangaroo (*Macropus giganteus*). J Wildl Dis 49:143–151. https://doi.org/10.7589/2012-01-027.
13. Stalder K, Vaz PK, Gilkerson JR, Baker R, Whiteley P, Ficorilli N, Tatarczuch L, Portas T, Skogvold K, Anderson GA, Devlin JM. 2015. Prevalence and clinical significance of herpesvirus infection in populations of Australian marsupials. PLoS One 10:e0133807. https://doi.org/10.1371/journal.pone.0133807.
14. Smith JA, Wellehan JF, Jr, Pogranichniy RM, Childress AL, Landolfi JA, Terio KA. 2008. Identification and isolation of a novel herpesvirus in a captive mob of eastern grey kangaroos (*Macropus giganteus*). Vet Microbiol 129:236–245. https://doi.org/10.1016/j.vetmic.2007.11.019.
15. Portas T, Fletcher D, Spratt D, Reiss A, Holz P, Stalder K, Devlin J, Taylor D, Dobroszczyk D, Manning AD. 2014. Health evaluation of free-ranging eastern bettongs (*Bettongia gaimardi*) during translocation for reintroduction in Australia. J Wildl Dis 50:210–223. https://doi.org/10.7589/2013-08-202.
16. Amery-Gale J, Vaz PK, Whiteley P, Tatarczuch L, Taggart DA, Charles JA, Schultz D, Ficorilli NP, Devlin JM, Wilks CR. 2014. Detection and identification of a gammaherpesvirus in Antechinus spp. in Australia. J Wildl Dis 50:334–339. https://doi.org/10.7589/2013-07-165.
17. Dickson J, Hopkinson WI, Coackley W, Spence T, Fairfax R. 1980. Herpesvirus hepatitis in rat kangaroos. Aust Vet J 56:463–464. https://doi.org/10.1111/j.1751-0813.1980.tb02657.x.
18. Wilcox RS, Vaz P, Ficorilli NP, Whiteley PL, Wilks CR, Devlin JM. 2011. Gammaherpesvirus infection in a free-ranging eastern grey kangaroo (*Macropus giganteus*). Aust Vet J 89:55–57. https://doi.org/10.1111/j.1751-0813.2010.00662.x.
19. Vaz PK, Mahony TJ, Hartley CA, Fowler EV, Ficorilli N, Lee SW, Gilkerson JR, Browning GF, Devlin JM. 2016. The first genome sequence of a metatherian herpesvirus: macropodid herpesvirus 1. BMC Genomics 17:70. https://doi.org/10.1186/s12864-016-2390-2.
20. Boname JM, Lehner PJ. 2011. What has the study of the K3 and K5 viral ubiquitin E3 ligases taught us about ubiquitin-mediated receptor regulation? Viruses 3:118–131. https://doi.org/10.3390/v3020118.
21. Wilkie GS, Kerr K, Stewart JP, Studdert MJ, Davison AJ. 2015. Genome sequences of equid herpesviruses 2 and 5. Genome Announc 3(2):e00119-15. https://doi.org/10.1128/genomeA.00119-15.
22. Li Q, Turk SM, Hutt-Fletcher LM. 1995. The Epstein-Barr virus (EBV) BZLF2 gene product associates with the gH and gL homologs of EBV and carries an epitope critical to infection of B cells but not of epithelial cells. J Virol 69:3987–3994.
23. Heine P, Braun N, Sevigny J, Robson SC, Servos J, Zimmermann H. 2001. The C-terminal cysteine-rich region dictates specific catalytic properties in

chimeras of the ectonucleotidases NTPDase1 and NTPDase2. Eur J Biochem 268:364–373. https://doi.org/10.1046/j.1432-1033.2001.01896.x.
24. Zhao G, Droit L, Tesh RB, Popov VL, Little NS, Upton C, Virgin HW, Wang D. 2011. The genome of Yoka poxvirus. J Virol 85:10230–10238. https://doi.org/10.1128/JVI.00637-11.
25. McInnes CJ, Wood AR, Thomas K, Sainsbury AW, Gurnell J, Dein FJ, Nettleton PF. 2006. Genomic characterization of a novel poxvirus contributing to the decline of the red squirrel (*Sciurus vulgaris*) in the UK. J Gen Virol 87:2115–2125. https://doi.org/10.1099/vir.0.81966-0.
26. Hobbs M, Pavasovic A, King AG, Prentis PJ, Eldridge MD, Chen Z, Colgan DJ, Polkinghorne A, Wilkins MR, Flanagan C, Gillett A, Hanger J, Johnson RN, Timms P. 2014. A transcriptome resource for the koala (Phascolarctos cinereus): insights into koala retrovirus transcription and sequence diversity. BMC Genomics 15:786. https://doi.org/10.1186/1471-2164-15-786.
27. Lee S, Cho H-J, Park J-J, Kim Y-S, Hwang S, Sun R, Song MJ. 2007. The ORF49 protein of murine gammaherpesvirus 68 cooperates with RTA in regulating virus replication. J Virol 81:9870–9877. https://doi.org/10.1128/JVI.00001-07.
28. Lee S-Y, Sarkar S, Bhattarai S, Namasivayam V, De Jonghe S, Stephan H, Herdewijn P, El-Tayeb A, Müller CE. 2017. Substrate-dependence of competitive nucleotide pyrophosphatase/phosphodiesterase1 (NPP1) inhibitors. Front Pharmacol 8:54. https://doi.org/10.3389/fphar.2017.00054.
29. Lee SY, Fiene A, Li W, Hanck T, Brylev KA, Fedorov VE, Lecka J, Haider A, Pietzsch HJ, Zimmermann H, Sevigny J, Kortz U, Stephan H, Muller CE. 2015. Polyoxometalates—potent and selective ecto-nucleotidase inhibitors. Biochem Pharmacol 93:171–181. https://doi.org/10.1016/j.bcp.2014.11.002.
30. Karlin S, Mocarski ES, Schachtel GA. 1994. Molecular evolution of herpesviruses: genomic and protein sequence comparisons. J Virol 68:1886–1902.
31. Honess RW, Gompels UA, Barrell BG, Craxton M, Cameron KR, Staden R, Chang YN, Hayward GS. 1989. Deviations from expected frequencies of CpG dinucleotides in herpesvirus DNAs may be diagnostic of differences in the states of their latent genomes. J Gen Virol 70:837–855. https://doi.org/10.1099/0022-1317-70-4-837.
32. Li H, Roossinck MJ. 2004. Genetic bottlenecks reduce population variation in an experimental RNA virus population. J Virol 78:10582–10587. https://doi.org/10.1128/JVI.78.19.10582-10587.2004.
33. Sacristán S, Malpica JM, Fraile A, García-Arenal F. 2003. Estimation of population bottlenecks during systemic movement of tobacco mosaic virus in tobacco plants. J Virol 77:9906–9911. https://doi.org/10.1128/JVI.77.18.9906-9911.2003.
34. Yao QY, Tierney RJ, Croom-Carter D, Dukers D, Cooper GM, Ellis CJ, Rowe M, Rickinson AB. 1996. Frequency of multiple Epstein-Barr virus infections in T-cell-immunocompromised individuals. J Virol 70:4884–4894.
35. Srivastava G, Wong KY, Chiang AKS, Lam KY, Tao Q. 2000. Coinfection of multiple strains of Epstein-Barr virus in immunocompetent normal individuals: reassessment of the viral carrier state. Blood 95:2443–2445.
36. Walling DM, Brown AL, Etienne W, Keitel WA, Ling PD. 2003. Multiple Epstein-Barr virus infections in healthy individuals. J Virol 77:6546–6550. https://doi.org/10.1128/JVI.77.11.6546-6550.2003.
37. Beyari MM, Hodgson TA, Cook RD, Kondowe W, Molyneux EM, Scully CM, Teo CG, Porter SR. 2003. Multiple human herpesvirus-8 infection. J Infect Dis 188:678–689. https://doi.org/10.1086/377504.
38. Bell SA, Balasuriya UB, Gardner IA, Barry PA, Wilson WD, Ferraro GL, MacLachlan NJ. 2006. Temporal detection of equine herpesvirus infections of a cohort of mares and their foals. Vet Microbiol 116:249–257. https://doi.org/10.1016/j.vetmic.2006.05.002.
39. Meredith RW, Westerman M, Springer MS. 2009. A phylogeny of Diprotodontia (Marsupialia) based on sequences for five nuclear genes. Mol Phylogenet Evol 51:554–571. https://doi.org/10.1016/j.ympev.2009.02.009.
40. Bast BJ, Zhou LJ, Freeman GJ, Colley KJ, Ernst TJ, Munro JM, Tedder TF. 1992. The HB-6, CDw75, and CD76 differentiation antigens are unique cell-surface carbohydrate determinants generated by the beta-galactoside alpha 2,6-sialyltransferase. J Cell Biol 116:423–435. https://doi.org/10.1083/jcb.116.2.423.
41. Liu Z, Swindall AF, Kesterson RA, Schoeb TR, Bullard DC, Bellis SL. 2011. ST6Gal-I regulates macrophage apoptosis via alpha2-6 sialylation of the TNFR1 death receptor. J Biol Chem 286:39654–39662. https://doi.org/10.1074/jbc.M111.276063.
42. Jackson RJ, Hall DF, Kerr PJ. 1999. Myxoma virus encodes an alpha2,3-sialyltransferase that enhances virulence. J Virol 73:2376–2384.
43. Darby AC, McInnes CJ, Kjær KH, Wood AR, Hughes M, Martensen PM, Radford AD, Hall N, Chantrey J. 2014. Novel host-related virulence factors are encoded by squirrelpox virus, the main causative agent of epidemic disease in red squirrels in the UK. PLoS One 9:e96439. https://doi.org/10.1371/journal.pone.0096439.
44. Boutard B, Vankerckhove S, Markine-Goriaynoff N, Sarlet M, Desmecht D, McFadden G, Vanderplasschen A, Gillet L. 2015. The alpha2,3-sialyltransferase encoded by myxoma virus is a virulence factor that contributes to immunosuppression. PLoS One 10:e0118806. https://doi.org/10.1371/journal.pone.0118806.
45. Sansom FM. 2012. The role of the NTPDase enzyme family in parasites: what do we know, and where to from here? Parasitology 139:963–980. https://doi.org/10.1017/S003118201200025X.
46. Knowles AF. 2011. The GDA1_CD39 superfamily: NTPDases with diverse functions. Purinergic Signal 7:21–45. https://doi.org/10.1007/s11302-010-9214-7.
47. Robson SC, Sévigny J, Zimmermann H. 2006. The E-NTPDase family of ectonucleotidases: structure function relationships and pathophysiological significance. Purinergic Signal 2:409–430. https://doi.org/10.1007/s11302-006-9003-5.
48. Sansom FM, Riedmaier P, Newton HJ, Dunstone MA, Müller CE, Stephan H, Byres E, Beddoe T, Rossjohn J, Cowan PJ, d'Apice AJF, Robson SC, Hartland EL. 2008. Enzymatic properties of an ecto-nucleoside triphosphate diphosphohydrolase from *Legionella pneumophila*: substrate specificity and requirement for virulence. J Biol Chem 283:12909–12918. https://doi.org/10.1074/jbc.M801006200.
49. Firon A, Dinis M, Raynal B, Poyart C, Trieu-Cuot P, Kaminski PA. 2014. Extracellular nucleotide catabolism by the group B streptococcus ecto-nucleotidase NudP increases bacterial survival in blood. J Biol Chem 289:5479–5489. https://doi.org/10.1074/jbc.M113.545632.
50. Sansom FM, Robson SC, Hartland EL. 2008. Possible effects of microbial ecto-nucleoside triphosphate diphosphohydrolases on host-pathogen interactions. Microbiol Mol Biol Rev 72:765–781. https://doi.org/10.1128/MMBR.00013-08.
51. Zimmermann H, Zebisch M, Strater N. 2012. Cellular function and molecular structure of ecto-nucleotidases. Purinergic Signal 8:437–502. https://doi.org/10.1007/s11302-012-9309-4.
52. Yegutkin GG. 2008. Nucleotide- and nucleoside-converting ectoenzymes: important modulators of purinergic signalling cascade. Biochim Biophys Acta 1783:673–694. https://doi.org/10.1016/j.bbamcr.2008.01.024.
53. Javed R, Yarimizu K, Pelletier N, Li C, Knowles AF. 2007. Mutagenesis of lysine 62, asparagine 64, and conserved region 1 reduces the activity of human ecto-ATPase (NTPDase2). Biochemistry 46:6617–6627. https://doi.org/10.1021/bi700036e.
54. Atkinson B, Dwyer K, Enjyoji K, Robson SC. 2006. Ecto-nucleotidases of the CD39/NTPDase family modulate platelet activation and thrombus formation: potential as therapeutic targets. Blood Cells Mol Dis 36:217–222. https://doi.org/10.1016/j.bcmd.2005.12.025.
55. Wang TF, Ou Y, Guidotti G. 1998. The transmembrane domains of ectoapyrase (CD39) affect its enzymatic activity and quaternary structure. J Biol Chem 273:24814–24821. https://doi.org/10.1074/jbc.273.38.24814.
56. Leal DBR, Streher CA, Bertoncheli CDM, Carli LFD, Leal CAM, da Silva JEP, Morsch VM, Schetinger MRC. 2005. HIV infection is associated with increased NTPDase activity that correlates with CD39-positive lymphocytes. Biochim Biophys Acta 1746:129–134. https://doi.org/10.1016/j.bbamcr.2005.10.009.
57. Barat C, Martin G, Beaudoin AR, Sevigny J, Tremblay MJ. 2007. The nucleoside triphosphate diphosphohydrolase-1/CD39 is incorporated into human immunodeficiency type 1 particles, where it remains biologically active. J Mol Biol 371:269–282. https://doi.org/10.1016/j.jmb.2007.05.012.
58. Chen CJ, Hsu WL, Yang HI, Lee MH, Chen HC, Chien YC, You SL. 2014. Epidemiology of virus infection and human cancer. Recent Results Cancer Res 193:11–32. https://doi.org/10.1007/978-3-642-38965-8_2.
59. Longnecker R, Kieff E, Ji C. 2013. Epstein-Barr virus/replication and Epstein-Barr virus. *In* Knipe D, Howley PM, Cohen JI, Griffin DE, Lamb RA, Martin MA, Racaniello VR, Roizman B (ed), Fields virology, 6th ed. Lippincott Williams & Wilkins, Philadelphia, PA.
60. Dow DE, Cunningham CK, Buchanan AM. 2014. A review of human herpesvirus 8, the Kaposi's sarcoma-associated herpesvirus, in the pedi-

atric population. J Pediatr Infect Dis Soc 3:66–76. https://doi.org/10.1093/jpids/pit051.
61. Simas P, Efstathiou S. 1998. Murine gammaherpesvirus 68: a model for the study of gammaherpesvirus pathogenesis. Trends Microbiol 6:276–282. https://doi.org/10.1016/S0966-842X(98)01306-7.
62. Altschul SF, Gish W, Miller W, Myers EW, Lipman DJ. 1990. Basic local alignment search tool. J Mol Biol 215:403–410. https://doi.org/10.1016/S0022-2836(05)80360-2.
63. Boratyn GM, Camacho C, Cooper PS, Coulouris G, Fong A, Ma N, Madden TL, Matten WT, McGinnis SD, Merezhuk Y, Raytselis Y, Sayers EW, Tao T, Ye J, Zaretskaya I. 2013. BLAST: a more efficient report with usability improvements. Nucleic Acids Res 41:W29–W33. https://doi.org/10.1093/nar/gkt282.
64. Krogh A, Larsson B, von Heijne G, Sonnhammer EL. 2001. Predicting transmembrane protein topology with a hidden Markov model: application to complete genomes. J Mol Biol 305:567–580. https://doi.org/10.1006/jmbi.2000.4315.
65. Petersen TN, Brunak S, von Heijne G, Nielsen H. 2011. SignalP 4.0: discriminating signal peptides from transmembrane regions. Nat Methods 8:785–786. https://doi.org/10.1038/nmeth.1701.
66. Zhang Y. 2008. I-TASSER server for protein 3D structure prediction. BMC Bioinformatics 9:40. https://doi.org/10.1186/1471-2105-9-40.
67. Mocarski E. 2007. Comparative analysis of herpesvirus-common proteins. *In* Arvin A, Campadelli-Fiume G, Mocarski E, Moore PS, Roizman B, Whitley R, Yamanishi K (ed), Human herpesviruses: biology, therapy, and immunoprophylaxis. Cambridge University Press, Cambridge, United Kingdom.
68. Davison AJ. 2007. Comparative analysis of the genomes. *In* Arvin A, Campadelli-Fiume G, Mocarski E, Moore PS, Roizman B, Whitley R, Yamanishi K (ed), Human herpesviruses: biology, therapy, and immunoprophylaxis. Cambridge University Press, Cambridge, United Kingdom.
69. Longnecker R, Neipel F. 2007. Introduction to the human gammaherpesviruses. *In* Arvin A, Campadelli-Fiume G, Mocarski E, Moore PS, Roizman B, Whitley R, Yamanishi K (ed), Human herpesviruses: biology, therapy, and immunoprophylaxis. Cambridge University Press, Cambridge, United Kingdom.
70. Katoh K, Standley DM. 2013. MAFFT multiple sequence alignment software version 7: improvements in performance and usability. Mol Biol Evol 30:772–780. https://doi.org/10.1093/molbev/mst010.
71. Tom R, Bisson L, Durocher Y. 2008. Transfection of HEK293-EBNA1 cells in suspension with linear PEI for production of recombinant proteins. CSH Protoc 2008:pdb.prot4977. https://doi.org/10.1101/pdb.prot4977.
72. Elleman TC, Domagala T, McKern NM, Nerrie M, Lonnqvist B, Adams TE, Lewis J, Lovrecz GO, Hoyne PA, Richards KM, Howlett GJ, Rothacker J, Jorissen RN, Lou M, Garrett TP, Burgess AW, Nice EC, Ward CW. 2001. Identification of a determinant of epidermal growth factor receptor ligand-binding specificity using a truncated, high-affinity form of the ectodomain. Biochemistry 40:8930–8939. https://doi.org/10.1021/bi010037b.
73. Vaz PK, Hartley CA, Browning GF, Devlin JM. 2015. Marsupial and monotreme serum immunoglobulin binding by proteins A, G and L and anti-kangaroo antibody. J Immunol Methods 427:94–99. https://doi.org/10.1016/j.jim.2015.10.007.
74. Cogan EB, Birrell GB, Griffith OH. 1999. A robotics-based automated assay for inorganic and organic phosphates. Anal Biochem 271:29–35. https://doi.org/10.1006/abio.1999.4100.